Optical Properties

pH-Triggered SERS via Modulated Plasmonic Coupling in Individual Bimetallic Nanocobs

*Maneesh K. Gupta, Sehoon Chang, Srikanth Singamaneni, Lawrence F. Drummy, Ray Gunawidjaja, Rajesh R. Naik, and Vladimir V. Tsukruk**

Hybrid organic–inorganic nanostructures are a critical platform for a wide range of chemical and biological sensing applications.[1–3] Optical responses, such as Raman scattering and absorbance, serve as a signature for specific chemical groups and can be used for identification and quantification of analyte molecules.[4] Raman scattering, which is the quantized vibration signature of a molecule, can be enhanced when the molecule is subjected to the enhanced electromagnetic field caused by plasmon resonance in the vicinity of plasmonic nanostructures.[5–7] It is well known that the plasmon absorption (resonance condition) and electromagnetic coupling between metal nanoparticles can be tuned by external ambient, shape, dimensions, interparticle distance, and orientation.[8–10] Of special interest is the coupling of surface plasmon resonances (SPR) in adjacent metal nanostructures separated by nanoscale gaps, which can modulate the optical absorption through coupling of plasmonic resonances.[11] These nanoscale gaps between plasmonic nanoparticles are also of intense interest as the formation of "hot spots" caused by the intense electric fields present in the gaps has been seen to dramatically enhance Raman scattering, leading to extremely sensitive analyte-detection schemes.[5,12–18]

Recently, the development of active plasmonic nanostructures, which exhibit selectively and reversibly tunable optical properties, has become an intense area of interest, especially in the fields of bioimaging, as well as chemical and biological sensing.[19,20] The development of active plasmonic nanostructures has the potential to open a wide range of new possibilities beyond the simple tracking of biomolecules. For example, active plasmonic nanostructures and other quantum phenomena could be used to detect catalytic events, map chemical gradients, and changes in pH in situ.[21–24] This responsive behavior can be realized by functionalization of nanoparticles with active moieties, such as responsive polymers that can mediate SPR coupling by changing the spatial dimensions of interparticle gaps and aggregation. A number of physical phenomena that cause large dimensional changes in materials due to volume phase transformations can be utilized for the design of these nanostructures.[25–27] Nanostructures such as metal nanoparticles and quantum dots have been widely used to track and detect biomolecules in cells, tissues, and whole organisms.[28]

To date, the vast majority of these efforts have concentrated on active control of SPR through aggregation of nanoparticles or through changes in the surrounding dielectric medium.[29] Changes in the surrounding dielectric medium can be used to detect binding or adsorption of chemical or biological molecules on the particle surface and swelling of a grafted polymer layer in a solvent.[30,31] However, such changes are limited in the types of stimuli that can be used and binding of biomolecules is often accompanied by spontaneous and nonreversible aggregation of nanoparticles, precluding quantitative analysis of the optical response.

For instance, the controlled placement of nanoparticles in the vicinity of the proper surfaces was suggested by Minko et al. as an efficient path to create a responsive surface.[32] Zhao et al. have demonstrated controlled temperature and light activation of aggregation as a way to modulate optical properties.[33,34] In another study, Nie et al. have also demonstrated pH-controlled aggregation of Raman-encoded nanoparticles as a way to turn on and off surface-enhanced Raman scattering (SERS) activity.[35] The aggregation-based optical properties of nanoparticles have also been extended to detect the enzymatic activity of endonucleases and methyltransferases.[36] The major limitation of aggregation-based approaches is the requirement of high concentrations of nanoparticles so that aggregation can be induced. This restricts the versatility of this approach, especially in cases where it is difficult to deliver high concentrations of nanoparticles. Moreover, the reliance on uncontrolled nanoparticle aggregates precludes the utilization of this phenomenon for intracellular sensing platforms.

In this Communication, we demonstrate the pH-triggered SPR and SERS properties of silver nanowires functionalized with gold nanoparticles in both solution and dry states. In contrast with previous examples of such bimetallic nanocobs, we utilize here a responsive polyacrylic acid (PAA) nanocoating that acts as a linker between the nanoparticles and nanowire.[37] The pH-responsive nature of the PAA nanocoating, which is sensitive to the environmental pH,

M. K. Gupta, S. Chang, Prof. S. Singamaneni, Dr. R. Gunawidjaja, Prof. V. V. Tsukruk
School of Materials Science and Engineering
Georgia Institute of Technology
771 Ferst Dr. NW, Atlanta, GA 30332, USA
E-mail: Vladimir@mse.gatech.edu
Dr. L. F. Drummy, Dr. R. R. Naik
Materials and Manufacturing Directorate
Air Force Research Laboratory
2941 Hobson Way, WPAFB, OH 45433, USA

DOI: 10.1002/smll.201002169

small NANO MICRO

is employed to vary the separation distance between the gold nanoparticles and the silver nanowire and thus control plasmon coupling. Moreover, placing nanoparticles inside a polymer-gel layer in close proximity to the nanowire surface effectively prevents any potential aggregation of nanoparticles under variable environmental conditions, in contrast with regular nanoparticle solutions, which easily precipitate with changing conditions.

Remarkably, this phenomenon is observed not only in the wet state (reversible changes in solution) but also under dry ambient conditions, indicating that pH-induced changes in the wet PAA nanocoating are robust enough to maintain changes in the optical properties and morphology even in the dry state. To this end, high-resolution transmission electron microscopy (HRTEM) employed in this work reveals that the thickness of the dry PAA nanocoating in the collapsed state is approximately equal to the width of only two polymer backbones (≈0.9 nm). Unexpectedly, even after drying in high vacuum, the pH-treated, initially swollen PAA nanocoating had a thickness of 4 nm. Such dramatic morphological changes result in the appearance of broad SPRs, which is critical for the appearance of a large SERS phenomenon.

The hybrid bimetallic nanocob structures were prepared by a multistep assembly of positively charged gold nanoparticles, Au:4-dimethylaminopyridine (DMAP), onto PAA-coated negatively charged one-dimensional silver nanowires (Ag:COOH).[37,38] TEM and atomic force microscopy (AFM) images show the length of Ag nanowires to be 6 ± 2 μm with a diameter of D = 75 ± 20 nm, aspect ratio of 80, and the characteristic grainy-surface morphology of bimetallic nanowires with gold nanoparticles surrounding silver nanowire, as shown in **Figure 1**a and the Supporting Information (SI). From the HRTEM images, the diameter of the spherical Au nanoparticles attached to the Ag nanowires was found to be 4.1 ± 1 nm (Figure 1b). HRTEM images confirm the crystal structure of the Au nanoparticle with 0.23 nm corresponding the (111) lattice spacing (Figure 1b).[39]

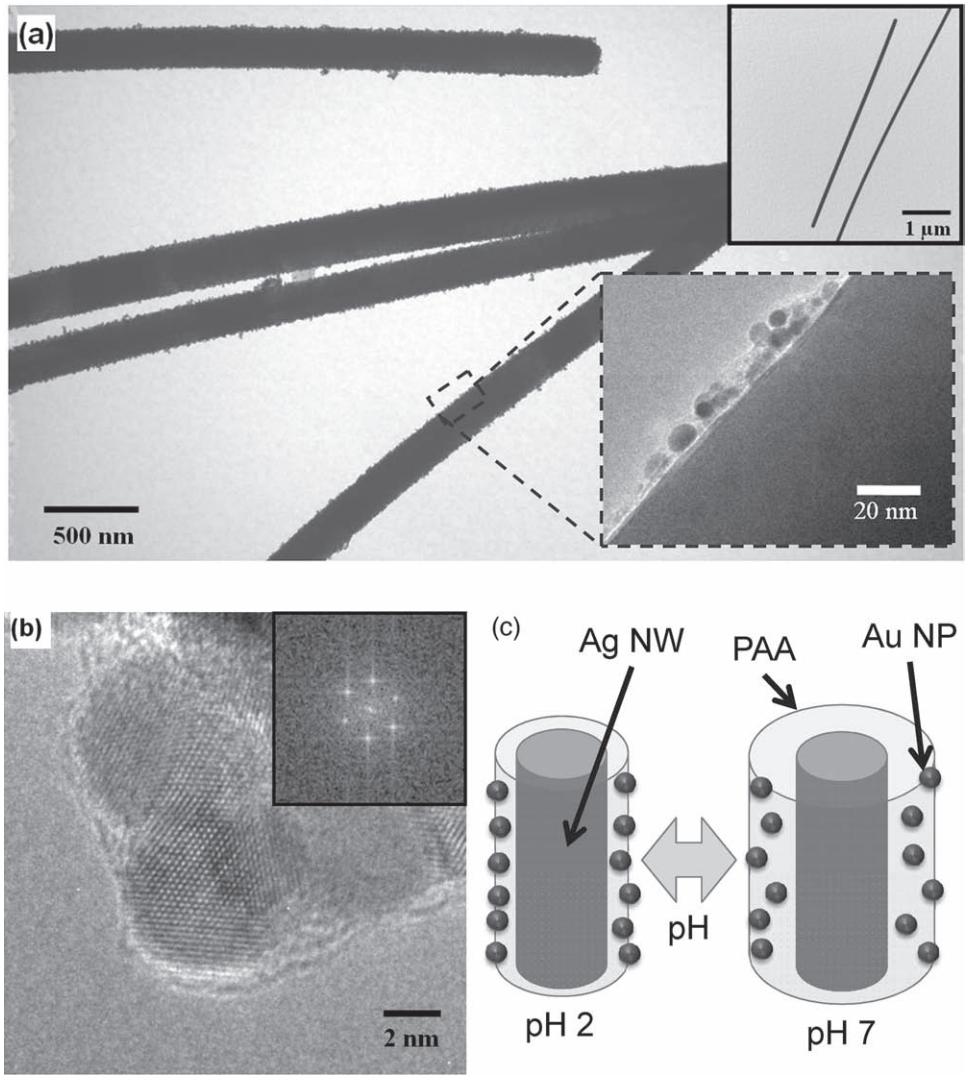

Figure 1. Structure of responsive nanocobs: a) TEM images of the nanocobs. The top inset shows a low-magnification view and the bottom inset shows a high-resolution image of the Au nanoparticles on the Ag nanowire. b) HRTEM image of Au nanoparticles (inset shows Fourier transform). c) Schematic depicting how pH-triggered changes in PAA thickness lead to variable interparticle distances.

The PAA nanocoating serves two important purposes in the fabrication of bimetallic nanocobs. Firstly, the PAA layer stabilizes the hybrid nanostructures in the solution, which otherwise tend to form irreversible aggregates that precipitate quickly. The PAA-coated nanocobs are very stable in aqueous solution; however, due to the large size of the nanowires they settle due to gravitational forces after several hours. Even after settling, the nanowires are easily dispersed by mild sonication. No irreversible aggregates were observed even after centrifugation of the nanocobs or storage of the samples for several months. Secondly, PAA, which is a weak anionic polyelectrolyte, imparts novel pH-responsive properties to the bimetallic hybrid nanocobs (Figure 1c). It is well known that, at neutral pH, the PAA takes on a highly swollen state. Deprotonated carboxylic groups cause an influx of counter ions and hence dramatic swelling (factor of 5–10 in linear dimension) of the polymer layer.[40] However, the PAA coating collapses at lower pH upon protonation of the carboxylic acid side group at pH values above 3.6.[40] Here, we suggest that this swelling–deswelling volume transition at pH 3.6 can be used to drive the plasmonic-coupling phenomena in the bimetallic nanocob (Figure 1c).

Complex UV–vis spectra for the assembled bimetallic nanocobs in solution reveal the presence of individual SPR peaks and variable coupling contributions at pH 2 and pH 7 (**Figure 2**). The UV–vis spectra of the component solutions show a characteristic silver-nanowire SPR peak at 390 nm and a characteristic SPR peak at 533 nm for individual gold nanoparticles.[38] The electron-energy-loss spectroscopy (EELS) spectrum of adsorbed bimetallic nanocobs shows a peak at 3.3 eV corresponding to an approximate wavelength of 375 nm, thus confirming an intact silver surface after modification, adsorption, and drying (see the SI).

The deconvolution of the UV–vis spectra for assembled nanocobs in solution clearly reveals four major contributing peaks: the first peak below 400 nm belongs to silver nanowires, the second peak within 500–550 nm represents SPR for individual gold nanoparticles, and smaller peaks within 700–850 nm are caused by SPR resonances originating from coupling of gold–gold and gold–silver nanostructures.[9,37] Comparison of UV–vis spectra at different pH reveals a significant redshift in the SPR peak of gold nanoparticles from 525 nm at pH 7 to 550 nm at pH 2. The SPR peak due to the coupling of gold and silver components also exhibits a redshift from 700 to 730 nm. Both shifts indicate increased plasmon coupling between gold nanoparticles and between gold nanoparticles and silver nanowires, which causes the dramatic appearance of SERS (see below). These changes can be attributed to both a variation in the surrounding dielectric caused by swelling of the PAA coating and to a change in plasmon coupling between the Au nanoparticles and the Ag nanowires.

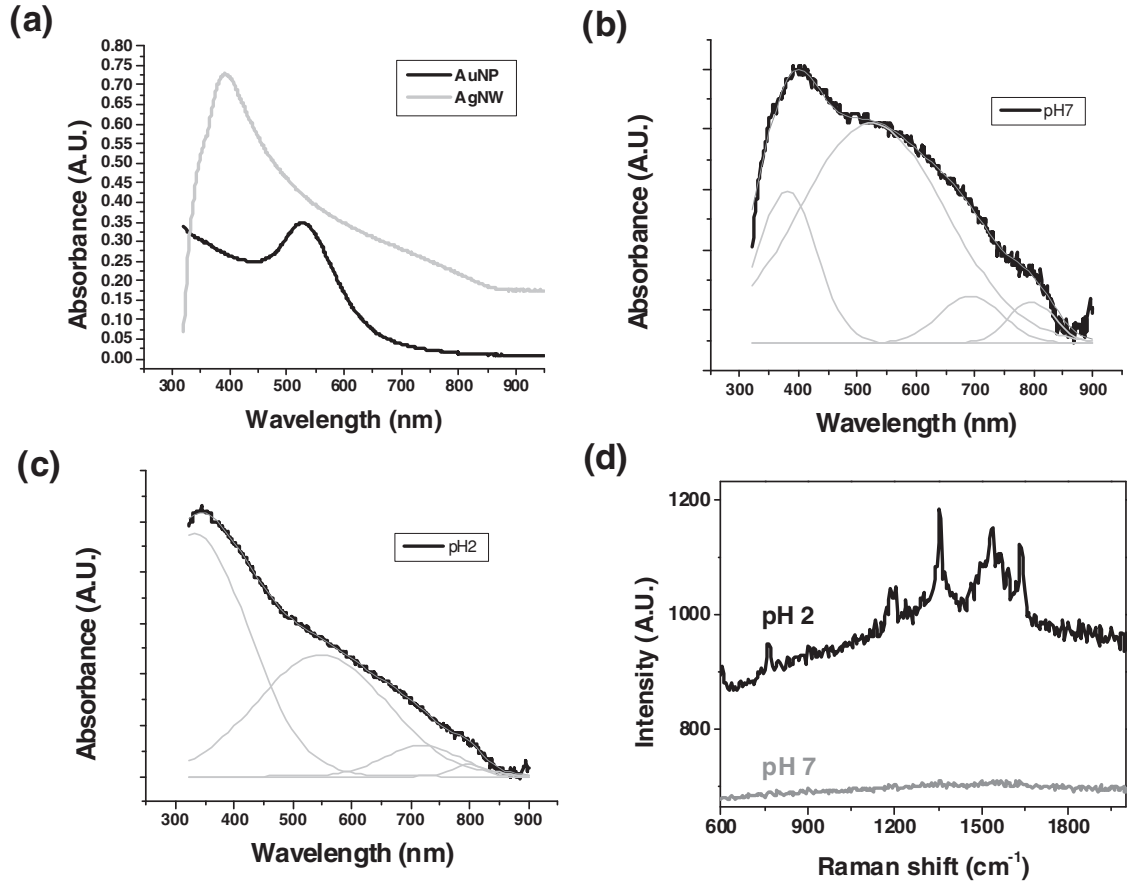

Figure 2. a) UV–vis spectra of solutions with Au nanoparticles and Ag nanowires. b) UV–vis spectrum of a solution of bimetallic nanocobs at pH 7. c) UV–vis spectrum of a solution of bimetallic nanocobs at pH 2; d) Raman spectra of R6G adsorbed on a single nanocob at pH 2 and pH 7.

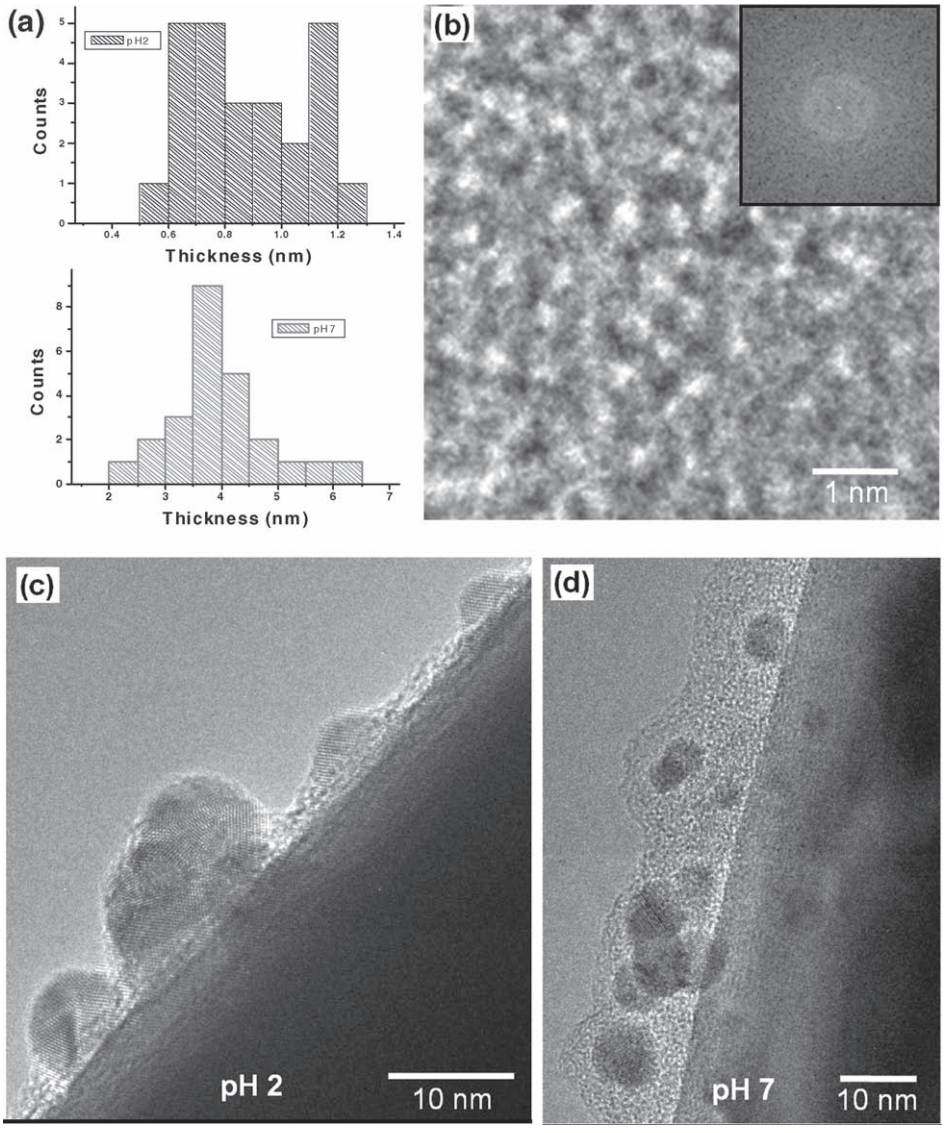

Figure 3. HRTEM analysis of bimetallic nanocobs. a) Total thickness of PAA nanocoating from individual nanocobs cast from at pH 2 and pH 7. b) HRTEM images showing a PAA layer on Ag nanowire at pH 7 (inset: corresponding Fourier transform). HRTEM images of a nanocob surface at pH c) 2 and d) 7 showing changes in polymer thickness and interparticle distance.

In order to verify how the observed changes in UV–vis spectra and SERS enhancement correlate with structural reorganizations, the morphology in the vicinity of the silver surfaces was monitored using HRTEM. Probing the structural changes in the ultrathin (2–5 nm) PAA nanocoating wrapped around the nanowires is extremely technically challenging. Conventional approaches for monitoring changes in the coating thickness, such as ellipsometry and AFM, cannot be readily applied in this case. As we find that the observed changes in the UV–vis and SERS enhancement persist even in the dry state, it is critical to experimentally determine structural features in the dry nanocobs. Dry-state samples were prepared for HRTEM by depositing 2 μL of dilute aqueous nanocob solution at either pH 2 or pH 7 directly on lacey carbon-coated TEM grids and the solution was allowed to dry at ambient conditions. Concentrated HCl was used to adjust the pH of the nanocob solution to pH 2 as measured by a digital pH meter. The pH 7 samples were deposited directly from 18.2 MΩ cm water without any additional treatment.

Indeed, the HRTEM images clearly reveal dramatic changes in the morphology of the PAA nanocoating on nanocobs adsorbed from solutions with different pHs (**Figure 3**). Firstly, at acidic conditions (collapsed state), the total thickness of the PAA nanocoating was found to be 0.88 ± 0.19 nm (Figure 3a). In contrast, the same PAA nanocoating at pH 7 was found to be 3.95 ± 0.33 nm. It is important to note that a four-fold change in the PAA thickness is observed here in the highly dried state in contrast to conventional observations in the wet state.[41] We suggest that the very significant differences in the thickness of the PAA layer, even in the dry state, is due to rapid drying of the nanocobs after deposition and the maintenance of acidic pH during the deposition and drying process. Since dilute aqueous HCl solutions are known to have vapor pressures and boiling points very similar to that

of pure water, it is expected that, while the local pH may vary slightly, an acidic pH below the pKa of 3.6 for PAA would be maintained throughout the drying process.

The internal morphology of the PAA nanocoating of silver nanowires cast from solutions with different pH was revealed by HRTEM (Figure 3). After drying from acidic conditions, the PAA nanocoating is highly collapsed and it is impossible to reveal the detailed morphology of collapsed polymer chains (Figure 3c). However, at pH 7, large PAA regions (up to 10 nm × 10 nm) can be found in the expanded state of continuous coatings despite the fact that the specimens were in the dry state, an unexpected result even for gel materials. This expanded state allowed for observation of the molecular ordering in the swollen-dried state (Figure 3b,d). The HRTEM image shows randomly varied contrast (bright and dark areas), which can be related to the presence of the amorphous PAA phase. The question of whether the observed expanded state can be associated with nanopores formation/preservation under the confined state of the nanoscale coating with embedded nanoparticles and the exact nature of the unusual phenomenon observed here remain to be elucidated. The Fourier transform shows a diffuse halo usually arising from liquid-like, short-range molecular ordering, a characteristic of amorphous polymer phases with or without porous morphologies. However, the exact location of this halo in reciprocal space is variable depending on the defocus value of the objective lens in HRTEM with further analysis required for conclusive discussion on the nature of the nanoscale morphology observed here.[42] It is difficult to make such local-density measurements from local variation of the phase contrast of HRTEM images of gel nanocoatings. However, alternative imaging techniques to quantitatively determine local density are currently underway.

The change in the separation of the gold nanoparticles and the silver surface is caused by the expanded state of the PAA layer (Figure 3). At pH 2, the distances evaluated from HRTEM images vary widely but stay below 1 nm, indicating almost direct contact of gold nanoparticles and silver nanowires (Figure 3a). In contrast at pH 7, swelling of the PAA layer results in many of the gold nanoparticles appearing to be lifted off the silver surface. The average distance between the gold nanoparticles and silver surface increases to above 3 nm. We suggest that the formation of such a wide gap, as compared to optimal gap size of within 1–2 nm, compromise the plasmon coupling and diminish the appearance of a strong SERS phenomenon.[11]

To verify how the reorganization of local morphology observed with HRTEM affects critical optical properties such as the SERS phenomenon, a known Raman marker, R6G, was employed as a model analyte (Figure 2d).[43,44] While the PAA polymer is also present in the metal/metal gap, the Raman scattering of R6G is much stronger than that of PAA and is dominant in the Raman spectra. Characteristic peaks from PAA that are reported in the literature are apparently not SERS active because they do not appear in any of the spectra obtained.[45] The SERS-peak assignment of R6G adsorbed on colloidal silver correspond to the literature data: 614 cm^{-1} is C–C–C ring in-plane bending; 774 and 1129 cm^{-1} are C–H in-plane bending; and 1183, 1310, 1363, 1509, 1572, and 1648 cm^{-1} are aromatic C–C stretches.[43] Nanocob solutions were exposed to 10^{-6} M R6G at pH 7. Excess R6G was washed before the solutions were adjusted to pH 2. Raman spectra were collected from a selected surface area that included only a single bimetallic nanocob deposited on a silicon surface. Care was taken to ensure that the polarization direction was normal to the long axis of the nanocob as this has been shown to have a strong influence on the intensity of SERS enhancement in coupled nanoparticle–nanowire systems.[46,47] At pH 7, the Raman spectrum for R6G has a very low intensity observed by the barely visible peaks (Figure 2d). In contrast, the Raman spectra for a single bimetallic nanocob cast from pH 2 solution shows similar R6G peaks but with increased intensity (more than two orders of magnitude) (Figure 2d). All peaks are sharp, well defined, and intense thus indicate a strong SERS enhancement after PAA nanocoating collapse to a very thin (<1 nm) coating at pH 2.

In conclusion we have demonstrated a bimetallic hybrid nanostructure assembled from gold nanoparticles embedded into a responsive PAA nanocoating around silver nanowires in which modulation of the gold–silver structural distances can serve as a chemical trigger for SERS activity. These finding are unique in that the modulation of the optical Raman signal occurred without uncontrolled interparticle aggregation but only through changes in the interparticle distances within a single nanocob complex. The tunable separation distance between the two plasmonic nanostructures resulted in modulation of electromagnetic coupling and thus a dramatic change in the corresponding SERS enhancement. The observed optical properties are reversible in wet state and can be presented in the dry state.

We suggest that the ability to change the optical and SERS properties of a single nanostructure is a significant advancement over the current approach involving aggregation of multiple nanoparticles by allowing measurements to be made independently of nanoparticle concentration and under robust conditions. Placing nanoparticles inside a polymer-gel layer in close proximity to the nanowire surface suggested here effectively prevents any potential aggregation of nanoparticles under variable environmental conditions, in contrast with regular nanoparticle solutions, which easily precipitate with even a slight change in environmental conditions (temperature, ionic conditions, pH, and shelf time). Future directions must focus on increasing the versatility of such complexes by the incorporation of polymers that are responsive to a wider array of and more practically important triggers, including temperature, light, electric field, and the presence of chemical or biological analytes. Also of great importance is an improved path for the fabrication of complexes with more homogeneous morphology, yielding stronger optical shifts, and systems such as nanoforests capable of multiplexed detection. Nanoparticle complexes designed with the basic principles described in this work have the potential to play a significant role in chemical and biological sensing applications that can be expanded to a wide variety of extreme environmental conditions, such as in-field, long-term, intracellular, or in vivo applications.

small NANO MICRO

Experimental Section

All chemicals were acquired from Sigma-Aldrich, Alfa-Aesar, VWR, and Fisher and used as received without further purification: silver nitrate salt (99.97%), poly(vinylpyrrolidone) (PVP; M_n = 1 300 000 Da), ethylene glycol (99%), $Fe(acac)_3$, poly(allylamine hydrochloride) (PAH; M_n = 70 000 g mol^{-1}), PAA (M_n = 100 000 g mol^{-1}, 35 wt% solution), transparent phosphate buffer (pH 7, 0.05 M), R6G, and dimethylformamide (ACS reagent grade). Silver nanowires[48,49] and gold nanoparticles[50] were synthesized in high yield according to standard procedures. In the procedures described below, 2 mg mL^{-1} PAA solution in pH 7 phosphate-buffered solution (0.01 M) is used for modification. All associated glassware were cleaned with aqua regia solution (3:1 HCl:HNO_3) and rinsed abundantly with nanopure water.

Silver-Nanowire Synthesis: A 60 mL solution of poly(vinylpyrrolidone) (PVP; 0.36 M) in ethylene glycol was heated at 160 °C under constant stirring for 1 h to remove water from the solution. Next, a separate 30 mL solution of silver nitrate in ethylene glycol ($AgNO_3$, 0.12 M) was prepared at room temperature by vigorous vortexing.[41] Sonication or heating was avoided, since it could lead to the unwanted formation of silver nanoparticles. Next, 50 μg of $Fe(acac)_3$ in 0.5 mL ethylene glycol solution was added into the hot PVP solution, followed by dropwise addition of the homogeneous silver nitrate solution. The drop-wise addition was done manually by means of pipette. The solution mixture was allowed to stir for a minimum of 1 h or until the solution turned opaque gray. The formation of silver nanowires could be easily confirmed from optical microscopy with 20× or 50× objectives in the dark-field mode.

4-DMAP-Coated Gold-Nanoparticle Synthesis: 4.1 mL aqueous solution of gold chloride ($HAuCl_4$·HCl; 30 mM) was mixed with 6.8 mL toluene solution of tetraoctylammonium bromide (TOAB; 25 mM) and vigorously stirred. As soon as all of the gold chloride salt has transferred from the aqueous phase into the organic phase, as seen from the distinctive yellow-orange color, a freshly prepared 4.1 mL ice-cold aqueous solution of sodium borohydride ($NaBH_4$; 0.4 M) solution is added dropwise into the two-phase solution mixture. The solution mixture gradually turns dark purple, almost black, accompanied by vigorous bubbling. The final solution mixture is left to stir overnight. The next day, the purple organic phase is extracted using a pipette and washed with 0.1 M sulfuric acid, followed by washing with 0.1 M sodium hydroxide, and finally is washed three times with nanopure water. Equal volume of an aqueous solution of 4-DMAP (0.1 M) is then added to the gold nanoparticles solution. Within 1 h, the gold nanoparticles moved into the aqueous phase. The aqueous phase is pipetted out and separated from the organic phase to give Au:DMAP solution.

Attachment of Gold Nanoparticles Onto Silver Nanowires: A certain amount of the methanolic solution of silver nanowires can be easily isolated from its solution by brief centrifugation at 3300 rpm for <5 min. Following the centrifugation in preweighed centrifuge tubes, the transparent supernatant is pipetted out to remove spherical nanoparticles. A typical concentration used for the subsequent procedure is 1–3 mg mL^{-1}.

To obtain negatively charged silver nanowires, 10 mg of silver nanowires is mixed with cysteamine ($NH_2CH_2CH_2SH$) overnight at a 1:10 mole ratio between the silver atom and cysteamine in methanol at a concentration of 0.5 mg mL^{-1}. The modified silver nanowires were isolated from excess ligands by multiple centrifugation–redispersion cycle in methanol. Finally, the silver nanowires are stored at pH 7 in phosphate buffer solution to activate the surface charge (1 mg mL^{-1}concentration, 10^{-5} M phosphate buffer). Silver nanowires are dispersible in the pH 7 buffer solution when sonicated or vortexed but gradually precipitate within 30 min. The silver nanowires are then redispersed in a PAA solution (2 mg mL^{-1}, 0.01 M phosphate buffer) with the aid of brief sonication and vortexing (0.5 mg mL^{-1} concentration).

The gold nanoparticle densities on silver nanowire substrates are varied as follows. To obtain low-density gold nanoparticles, a 0.1 mL solution of the as-prepared Au:DMAP solution is diluted in a 2.4 mL nanopure water (pH 7, 2×10^{-3} M phosphate buffer). Next, this solution mixture is added dropwise into a stirring solution of 2.5 mL of negatively charged silver nanowires (1 mg mL^{-1} concentration, pH 7, 2×10^{-3} phosphate buffer). The solution mixture is sonicated for 30 s and vortexed for 2 min to ensure uniform attachment of gold nanoparticles onto the silver-nanoparticle surface. Any excess of unattached gold nanoparticles is then removed by centrifugation (3300 rpm, 5 min). The silver-nanowire–gold-nanoparticle nanostructures are then redispersed in PAA solution (2 mg mL^{-1}, 0.01 M phosphate buffer) with the aid of brief sonication and vortexing (0.5 mg mL^{-1} concentration). Excess of unattached PAA is removed with multiple centrifugation and redispersion cycles in nanopure water. This is to coat the outer silver–gold nanostructure with PAA. Otherwise, the silver–gold nanoparticles are not dispersible in water. For high-density gold nanoparticles, a 0.5 mL solution of the as-prepared Au:DMAP solution is used instead for the same amount of silver nanoparticles. Correspondingly, five-fold phosphate-buffer concentration is used.

Characterization: The nanocob solutions were adjusted to pH 2 by drop-wise addition of concentrated HCl. The pH of the solution was monitored using a digital pH meter. UV–vis spectra of nanocob solutions at pH 7 and 2 were recorded using a Shimadzu UV-2450 spectrophotometer. Samples were prepared for dry-state characterization (AFM, HRTEM, and Raman spectroscopy) by depositing 2 μL of nanocob solution on either lacey carbon-coated TEM grids or freshly piranha-cleaned silicon substrates. The solution was allowed to dry at ambient conditions. AFM topographical and phase images were obtained using a Dimension-3000 microscope in the tapping mode at 1.0–2.0 Hz scan rate, according to the usual procedure.[51,52] HRTEM images and EELS spectra were collected using a 300 kV FEI Titan microscope equipped with a C_s image corrector and a Gatan Imaging Filter (GIF) Tridiem.

Raman spectra were collected with an Alpha300R Witek confocal Raman microscope with Argon ion laser (λ = 514.5 nm) with the incident power set below 3 mW and 20 s integration time.[53] The samples are prepared for Raman measurements by first exposing the wires to 10^{-6} M R6G at neutral pH. Excess R6G is then removed by centrifuging the nanocobs and rinsing with water. Following removal of the excess R6G, the pH of the samples was adjusted to pH 2 as described above.

Supporting Information

Supporting Information is available from the Wiley Online Library or from the author.

Acknowledgements

This work was supported by the AROSR Grant FA9550-08-1-0446, by the AFRL/GT BIONIC Center (FA 9550-09-1-0162), and also by the NSF Grant CBET-093078.

[1] C. A. Mirkin, R. L. Letsinger, R. C. Mucic, J. J. Storhoff, *Nature* **1996**, *382*, 607–609.
[2] J.-M. Nam, C. S. Thaxton, C. A. Mirkin, *Science* **2003**, *301*, 1884–1886.
[3] T. Vo-Dinh, A. Dhawan, S. J. Norton, C. G. Khoury, H.-N. Wang, V. Misra, M. D. Gerhold, *J. Phys. Chem. C* **2010**, *114*, 7480–7488.
[4] J. N. Anker, W. P. Hall, O. Lyandres, N. C. Shah, J. Zhao, R. P. Van Duyne, *Nat. Mater.* **2008**, *7*, 442–453.
[5] H. Ko, S. Singamaneni, V. V. Tsukruk, *Small* **2008**, *4*, 1576–1599.
[6] P. K. Jain, K. S. Lee, I. H. El-Sayed, M. A. El-Sayed, *J. Phys. Chem. B* **2006**, *110*, 7238–7248.
[7] R. A. Alvarez-Puebla, L. M. Liz-Marzan, *Energy Environ. Sci.* **2010**, *3*, 1011–1017.
[8] W. A. Murray, W. L. Barnes, *Adv. Mater.* **2007**, *19*, 3771–3782.
[9] C. Jiang, S. Markutsya, V. V. Tsukruk, *Langmuir* **2004**, *20*, 882–890.
[10] R. A. Alvarez-Puebla, L. M. Liz-Marzán, *Small* **2010**, *6*, 604–610.
[11] P. K. Jain, W. Huang, M. A. El-Sayed, *Nano Lett.* **2007**, *7*, 2080–2088.
[12] H. Xu, E. Bjerneld, M. Käll, L. Börjesson, *Phys. Rev. Lett.* **1999**, *83*, 4357–4360.
[13] H. Xu, J. Aizpurua, M. Käll, P. Apell, *Phys. Rev. E* **2000**, *62*, 4318–4324.
[14] H. Xu, X.-H. Wang, M. Persson, H. Xu, M. Käll, P. Johansson, *Phys. Rev. Lett.* **2004**, *93*, 243002.
[15] Y. Lu, L. G. Liu, L. P. Lee, *Nano Lett.* **2005**, *5*, 5–9.
[16] C. E. Talley, J. B. Jackson, C. Oubre, N. K. Grady, C. W. Hollars, S. M. Lane, T. R. Huser, P. Nordlander, N. J. Halas, *Nano Lett.* **2005**, *5*, 1569–1574.
[17] S. Chang, H. Ko, S. Singamaneni, R. Gunawidjaja, V. V. Tsukruk, *Anal. Chem.* **2009**, *81*, 5740–5748.
[18] H. Ko, V. V. Tsukruk, *Small* **2008**, *4*, 1980–1984.
[19] J. E. Ghadiali, M. M. Stevens, *Adv. Mater.* **2008**, *20*, 4359–4363.
[20] V. Kozlovskaya, E. Kharlampieva, B. P. Khanal, P. Manna, E. R. Zubarev, V. V. Tsukruk, *Chem. Mater.* **2008**, *20*, 7474–7485.
[21] Y. B. Zheng, T. J. Huang, *J. Assoc. Lab. Autom.* **2008**, *13*, 215–226.
[22] V. K. S. Hsiao, Y. B. Zheng, B. K. Juluri, T. J. Huang, *Adv. Mater.* **2008**, *20*, 3528–3532.
[23] Y. B. Zheng, Y.-W. Yang, L. Jensen, L. Fang, B. K. Juluri, A. H. Flood, P. S. Weiss, J. F. Stoddart, T. J. Huang, *Nano Lett.* **2009**, *9*, 819–825.
[24] E. Kharlampieva, V. Kozlovskaya, O. Zavgorodnya, G. D. Lilly, N. A. Kotov, V. V. Tsukruk, *Soft Matter* **2010**, *6*, 800–807.
[25] M. A. C. Stuart, W. T. S. Huck, J. Genzer, M. Müller, C. Ober, M. Stamm, G. B. Sukhorukov, I. Szleifer, V. V. Tsukruk, M. Urban, F. Winnik, S. Zauscher, I. Luzinov, S. Minko, *Nat. Mater.* **2010**, *9*, 101–113.
[26] I. Luzinov, S. Minko, V. V. Tsukruk, *Prog. Polym. Sci.* **2004**, *29*, 635–698.
[27] I. Luzinov, S. Minko, V. V. Tsukruk, *Soft Matter* **2008**, *4*, 714–725.
[28] M. De, P. S. Ghosh, V. M. Rotello, *Adv. Mater.* **2008**, *20*, 4225–4241.
[29] J. A. Schuller, E. S. Barnard, W. Cai, Y. C. Jun, J. S. White, M. L. Brongersma, *Nat. Mater.* **2010**, *9*, 193–204.
[30] C. J. Murphy, A. M. Gole, S. E. Hunyadi, J. W. Stone, P. N. Sisco, A. Alkilany, B. E. Kinard, P. Hankins, *Chem. Commun.* **2008**, 544–557.
[31] B. Sepulveda, P. C. Angelome, L. M. Lechuga, L. M. Liz-Marzan, *Nano Today* **2009**, *4*, 244–251.
[32] I. Tokarev, I. Tokareva,S. Minko, *Adv. Mater.* **2008**, *20*, 2730–2734.
[33] A. Housni,Y. Zhao, Y. Zhao, *Langmuir* **2010**, *26*, 12366–12370.
[34] A. Housni, Y. Zhao, *Langmuir* **2010**, *26*, 12933–12939.
[35] X. Qian, J. Li, S. Nie, *J. Am. Chem. Soc.* **2009**, *131*, 7540–7541.
[36] G. Song, C. Chen, J. Ren, X. Qu, *ACS Nano* **2009**, *3*, 1183–1189.
[37] R. Gunawidjaja, S. Peleshanko, H. Ko, V. V. Tsukruk, *Adv. Mater.* **2008**, *20*, 1544–1549
[38] R. Gunawidjaja, E. Kharlampieva, I. Choi, V. V. Tsukruk, *Small* **2009**, *5*, 2460–2466.
[39] R. Sakthivel, B. Das, B. Satpati, B. K Mishra, *Appl. Surf. Sci.* **2009**, *255*, 6577–6581.
[40] H. Kitano, Y. Akatsuka, N. Ise, *Macromolecules* **1991**, *24*, 42–46.
[41] O. E. Philippova, D. Hourdet, R. Audebert, A. R. Khokhlov, *Macromolecules* **1997**, *30*, 8278–8285.
[42] J. C. H. Spence, *High Resolution Electron Microscopy*, Oxford University Press, Oxford, UK **2003**, p. 295.
[43] P. Hildenbrandt, M. Stockburger, *J. Phys. Chem.* **1984**, *88*, 5935–5944.
[44] M. Michaels, L. Brus, *J. Phys. Chem. B* **2000**, *104*, 11965–11971.
[45] J. Dong, Y. Ozaki, K. Nakashima, *Macromolecules* **1997**, *30*, 1111–1117.
[46] H. Wei, F. Hao, Y. Huang, W. Wang, P. Nordlander, H. Xu, *Nano Lett.* **2008**, *8*, 2497–2502.
[47] Y. Fang, H. Wei, F. Hao, P. Nordlander, H. Xu, *Nano Lett.* **2009**, *9*, 2049–2053.
[48] B. Wiley,Y. Sun, Y. Xia, *Langmuir* **2005**, *21*, 8077–8080.
[49] A. Tao, F. Kim, C. Hess, J. Goldberger, R. He, Y. Sun, Y. Xia, P. Yang, *Nano Lett.* **2003**, *3*, 1229–1233.
[50] M. Brust, D. Bethell, D. J. Schiffrin, C. J. Kiely, *Adv. Mater.* **1995**, *7*, 795–797.
[51] V. V. Tsukruk, *Rubber Chem. Technol.* **1997**, *70*, 430.
[52] M. E. McConney, S. Singamaneni, V. V. Tsukruk, *Polym. Rev.* **2010**, *50*, 235–286.
[53] S. Singamaneni, M. Gupta, R. Yang, M. M. Tomczak, R. R. Naik, Z. L. Wang, V. V. Tsukruk, *ACS Nano* **2009**, *3*, 2593–2600.

Received: December 3, 2010
Revised: January 31, 2011
Published online: April 14, 2011

